

Preliminary studies of spherical proof masses in LISA drag-free satellites

Benjamin Lange*

August 29, 2002

ABSTRACT

The results of preliminary studies using a spherical proof mass in the LISA mission are given. These include the acceleration disturbance performance, methods for controlling and calibrating a spinning sphere, system considerations, the possibility of using the spinning reference as a precision gyroscope to improve the attitude control, and a preliminary design with a spherical proof mass.

1. INTRODUCTION

Operating a gravity-wave detector in space has a number of advantages including enhanced sensitivity and a very low-frequency (10^{-3} to 10^{-4} Hz) lower band edge. The Laser Interferometer Space Antenna, LISA, as currently planned will place three drag-free satellites separated by 5 million km in a solar orbit 20 degrees behind the earth. The space between the satellites will function as the arms of a laser interferometer with the drag-free proof masses acting as the interferometer mirrors. The low frequency limit of the detection band is limited by the accelerometer (specific force) noise of the proof masses, and in order to achieve a lower limit of 10^{-3} Hz, an acceleration noise of about 10^{-15} m/sec²/Hz^{1/2} is required. Because variations in the solar radiation generate an acceleration noise of about 10^{-10} m/sec²/Hz^{1/2}, a drag-free satellite¹ is required to shield the proof masses from direct sun light.

There are two possibilities for the proof masses. Either two single-axis cubes, each pointing at one of the neighboring satellites, or a single sphere reflecting the two beams may be used. This paper will discuss the design using a single spherical proof mass in each satellite.

2. SPHERICAL CONFIGURATION

A LISA satellite with a spherical proof mass would look much like the configuration with two single-axis cubical proof masses with the two cubes replaced by a single sphere. There would be an extra converging lens between the beams and the sphere to focus the four beams at the center of the sphere. When the sphere is centered with sufficient accuracy by the drag-free controller, the beams are reflected back out of the lenses as if from a planar surface. In order to keep the surface irregularities from appearing in the LISA band, the sphere must spin at one Hz or more and the angular velocity must be accurately damped to the sphere's maximum axis of inertia².

* blange@virtualpbx.com; phone 1 415 221 6600 x 310; fax 1 415 221 6600; <http://www.dragfreesatellite.com>; VirtualPBX.Com, 1922 Page Street, San Francisco, CA, USA 94117.

The position readout of the proof mass would be done with a 3-axis transcollimator³, and there would be 3 or 4 transcollimators to guarantee reliability. In addition to the transcollimators, a three-axis eddy-current spin-up motor would surround the sphere. The coils of the motor would resemble standard Helmholtz coils. Assuming a pointing requirement of 8×10^{-9} rad/Hz^{1/2}, the drag-free controller requirement would be 0.2×10^{-9} m/Hz^{1/2} for a sphere of radius 2.5 cm. This requirement comes from the angle error of reflection from a miscentered sphere.

3. TRANSCOLLIMATOR POSITION READOUT

A transcollimator is precision optical readout of the translation of a sphere. It is identical to a standard autocollimator with one exception, the collimating lens focuses the output beam to converge at the center of the sphere. When this is done the instrument becomes insensitive to rotation and a translation of the sphere perpendicular to the beam axis has the same effect as the rotation of the mirror in an autocollimator. If a laser is used for the light source, the third translation motion parallel to the beam can also be detected. This is a 3-axis transcollimator. The advantage of the 3-axis transcollimator is that a wide gap with low noise equivalent translation, i.e. high sensitivity, is possible.

If x is the translation of the sphere perpendicular to the beam, it is equivalent to the rotation angle, θ , of the mirror of an autocollimator given by $\theta = x / a$ where a is the radius of the sphere, see Figure 1. Using the Jones design for the transcollimator⁴, a noise equivalent translation of about 5×10^{-12} m / Hz^{1/2} is possible. The Jones reticle shown in Figure 2 solves the contradictory requirements of having a large number of photons and a narrow slit by using a grid of slits. The principle is illustrated in the single axis reticle. A translation of the sphere slides the image of the field-stop mask over the detector mask uncovering one side and covering the other. This unbalances the signals in the photodetectors and reads out the displacement. The total amount of light through slits is constant making it possible to also run a laser interferometer in the third (beam) axis. Also the light is evenly distributed over the entire photodetector surface. Although the figure only shows about 9 slits, the slits would typically be about 25 μ wide giving about 100 slits per 5 mm.

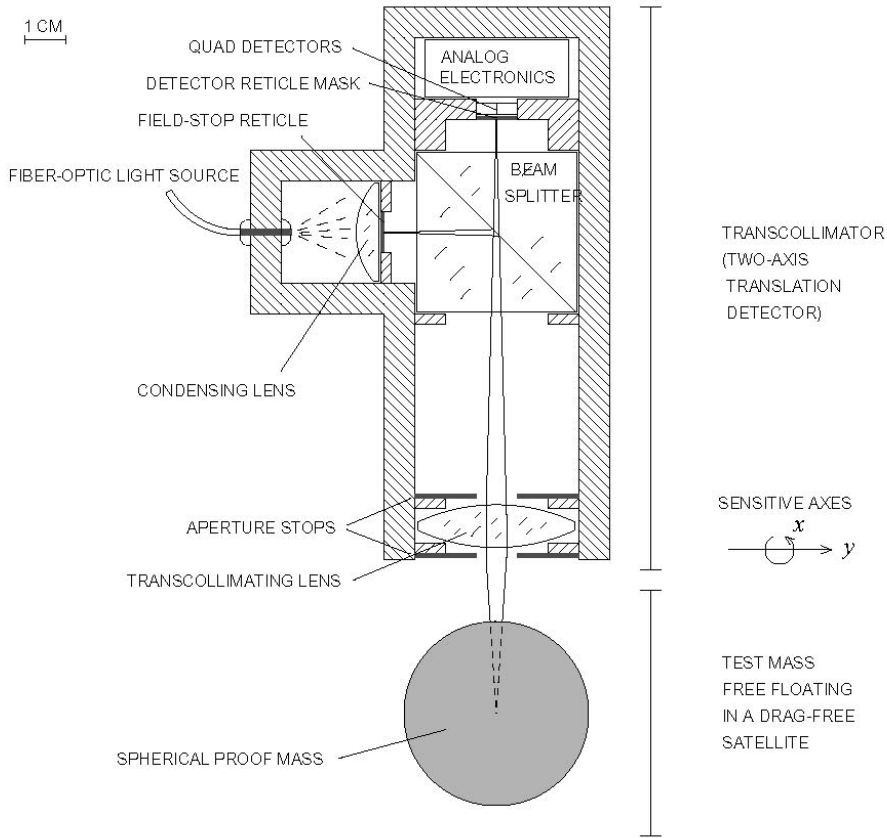
The instrument noise is very low, but if the spherical surface is not accurately polished, surface irregularities can give rise to transcollimator errors of equal size. The uncoated GP-B spheres have surface errors of about 20 nanometers, but spinning the sphere moves these errors out of the LISA band. In addition it is possible to calibrate a map of the spherical surface by supporting the sphere in an electric bearing, spinning it, and inducing a large polhode motion with an active damper⁵.

4. PERFORMANCE CALCULATIONS

The LISA acceleration performance with a spherical proof mass is summarized in Table 1 which is taken from [6]. The disturbances are divided into three categories:

- 1) Disturbances external to the spacecraft. These come from the interplanetary magnetic field and radiation of which the only important source is occasional solar flares.
- 2) Internal disturbances coupled to the relative motion of the spacecraft due to field gradients at the proof mass. These come from gravity, electric, and magnetic gradients and have been bounded by the DISCOS flight results⁷.
- 3) Internal disturbances which do not depend on the relative motion of the spacecraft. These include gas-molecule collisions from the residual vacuum, gravity-gradient variations from thermal fluctuations, photon shot noise from the detectors and discharge UV, and a radiometer-like effect from temperature fluctuations in the proof mass.

TRANSCOLLIMATOR DESIGN



TRANSCOLLIMATOR PRINCIPLE: CHANGE TRANSLATION INTO AN ANGLE AND READ THE ANGLE WITH A STANDARD AUTOCOLLIMATOR

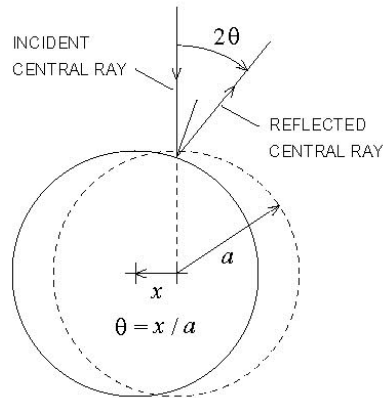


Figure 1. Transcollimator Optical Translation Detector

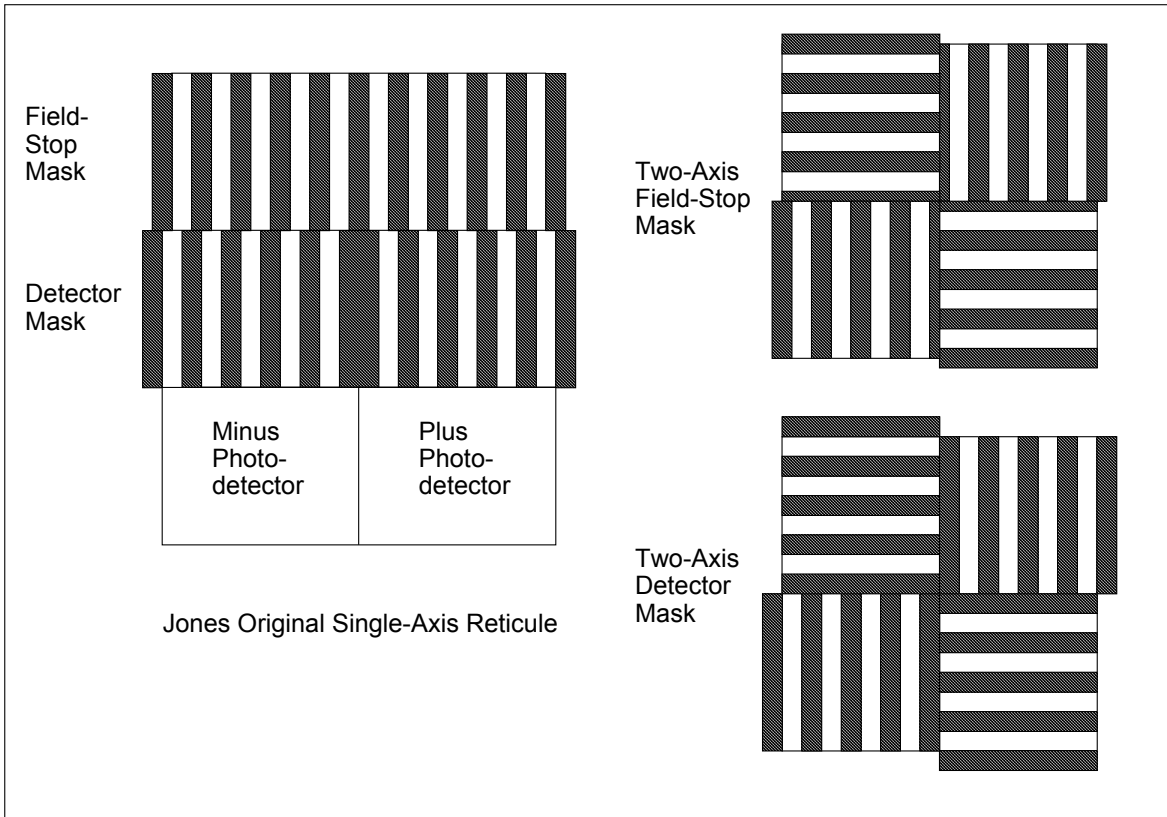


Figure 2. Single- and Two-Axis Jones-Pfund Type Reticules

5. EXTERNAL DISTURBANCES

Since the only significant radiation source is solar flares⁶ which are rare and can be removed from the data, the only important external disturbance is from the interplanetary magnetic field.

This has been measured by the Ulysses spacecraft⁸. This and other Ulysses data show that the interplanetary magnetic field power spectrum is $1/f^2$ with a peak of 10^4 nT²/Hz at 10^{-4} Hz, i.e. the root power spectrum is $1/f$ with a peak of 100 nT/Hz^{1/2} at 10^{-4} Hz. Because the theory of eddy currents in spinning conducting spheres is well understood⁹ and because of the Ulysses measurements, the external disturbances are well in hand.

6. INTERNAL DISTURBANCES COUPLED TO THE SPACECRAFT MOTION AND THE DISCOS BOUNDS

If it is desired to fly a high-accuracy drag-free satellite, it is best to spin the satellite about an axis perpendicular to the orbit plane; and the worst choice is locally-level attitude control¹. Also the proof mass should be accurately controlled to the reference position of the self-gravity calculations. DISCOS violated both of these criteria. The satellite attitude-

control was gravity-gradient stabilized and the control limit cycle was about one mm. What at the time seemed undesirable is now very fortunate. The worst choice for good drag-free performance is the best choice to measure the gradient fields in the cavity.

Because of this the DISCOS flight has demonstrated that no field gradient at the proof mass exceeded about $10^{-7} / \text{sec}^2$. When this is combined with the expected drag-free performance of LISA, $10^{-9} \text{ meters/Hz}^{1/2}$; the DISCOS flight has demonstrated $10^{-16} \text{ m/sec}^2/\text{Hz}^{1/2}$ for the internal disturbances which depend on spacecraft motion.

The implication is that a special mission to demonstrate the drag-free performance is not necessary, since it has already flown.

7. INTERNAL DISTURBANCES WHICH DO NOT DEPEND ON SPACECRAFT MOTION

The major internal disturbance which does not depend on spacecraft motion is the specific force spectrum caused by collisions from gas molecules due to the residual vacuum. This is about $0.12 \times 10^{-15} \text{ m/sec}^2/\text{Hz}^{1/2}$. This disturbance goes as the square root of pressure so even a major error in attaining the required vacuum would not have serious consequences.

The rest of the internal disturbances are very small so that an error in their estimation is unlikely to be important. Thus the conclusion is that these disturbances are also well in hand.

Source of Noise	Formulas	Auxiliary Formula, Critical Values, Comments, Etc.	Specific Force Noise
	DFS control = $10^{-9} \text{ m/Hz}^{1/2}$, $a = 2.5 \text{ cm}$, gap = 2 cm, $m_{PM} = 1.47 \text{ kg}$	$T = 300 \text{ K}$, $p = 10^{-9} \text{ Torr} = 1.33 \times 10^{-7} \text{ N/m}^2$, $\omega_{PM} = 6 \text{ rad/sec}$	Units $10^{-15} \text{ m/sec}^2/\text{Hz}^{1/2}$
Internal Magnetic Field Gradient	$\mathbf{f} = (\mathbf{m}_m \cdot \nabla) \mathbf{B}_{sc} / m_{PM}$	$m_m = 4.2 \times 10^{-9} \text{ Am}^2$, eddy currents. $B_{sc} = 100 \text{ nT/Hz}^{1/2}$ $m_m = 7.2 \times 10^{-11} \text{ Am}^2$, sus	2.8E-01 4.9E-03
Lorentz Force from Interplanetary Field	$\mathbf{f} = Sh q \mathbf{v}_o \times \mathbf{B}_{ip} / m_{PM}$	$Sh = 0.1$, $q = 6 \times 10^{-13} \text{ coul}$, $B_{ip} = 100 \text{ nT/Hz}^{1/2}$	1.3E-01
Electric Charge		$q = 6 \times 10^{-13} \text{ coul}$	3.2E-05
	Smythe, 5.08		
Delta T Fluctuations	Proof Mass T variations	$\Delta T_{PM} = 10^{-4} \text{ K/Hz}^{1/2}$	5.9E-02
Residual Gas	$\text{PSD} = 3 \frac{2d_g kT}{m_{PM}^2}$	$d_g = 3pa^2 \sqrt{\frac{2\pi m_{av}}{kT}}$	1.26E-01
Photon Gas	$\text{PSD} = 3 \frac{2d_g kT}{m_{PM}^2}$	$d_{ph} = 1.11h \frac{a^2}{\lambda_m^4}$	7.76E-04
Cosmic Rays	See text.		4.90E-04
Solar Flares	See text. Not in RSS.	Can be omitted from data.	4.90E-01
Thermal Gravity	DISCOS meas $\times \alpha \Delta T_{SC}$	$\Delta T_{SC} = 0.01 \text{ K/Hz}^{1/2}$	2.0E-04
Thermal Gravity Gradient		$\alpha = 4 \times 10^{-7} / \text{K}$	3.5E-02

Motion Gravity Gradient	$dg/dx = 3 \times 10^{-8} / \text{sec}^2$ from DISCOS meas and calc		3.0E-02
Transcollimator Light Pressure	$\text{PSD} = \frac{2h^2 n}{\lambda^2 m_{PM}^2} = \frac{2hP}{c\lambda m_{PM}^2}$	$n = 5 \times 10^{10}$ ph/sec $P = 10^{-8}$ watts, $\lambda = 10^{-6}$ m	5.72E-07
UV Discharge Light Pressure	$\text{PSD} = \frac{2h^2 n}{\lambda_{UV}^2 m_{PM}^2} = \frac{2hP_{UV}}{c\lambda_{UV} m_{PM}^2}$	$n = 6 \times 10^5$ ph/sec $P = 10^{-10}$ w, $\lambda_{UV} = 2 \times 10^{-7}$ m	2.52E-08
Interferometer Light Pressure	$\text{PSD} = \frac{2h^2 n_{Int}}{\lambda_{Int}^2 m_{PM}^2} = \frac{2hP_{Int}}{c\lambda_{Int} m_{PM}^2}$	$n_{Int} = 5 \times 10^{16}$ ph/sec $P_{Int} = 0.01$ w, $\lambda_{Int} = 10^{-6}$ m	1.43E-04
Laser Power Fluctuations	$sfn = \frac{2\Delta P_{Int}}{c m_{PM}}$	$\Delta P_{Int} = 5 \times 10^{-7} \times 0.01$ w	2.27E-02
Out-gassing Pumping Currents		No noise beyond residual gas.	
Large Particles		All large particles assumed trapped within 15 sec.	
	RSS of all sources	Units $10^{-15} \text{ m/sec}^2/\text{Hz}^{1/2}$	3.4E-01

Table 1. LISA Acceleration Error Budget for Spherical Free-Floating Proof Mass

8. ASSUMPTIONS AND NOTATION

The notation in Table 1 is

- a = Radius of proof mass = 2.5 cm.
- m_{PM} = Mass of the proof mass = 1.47 kg.
- ω_{PM} = Angular velocity of the proof mass in rad/sec = 6 rad/sec.
- m_m = Magnetic moment in Amp-meters.
- q = Electric charge on the proof mass in coulombs.
- \mathbf{f} = Specific force in $\text{m/sec}^2/\text{Hz}^{1/2}$.
- \mathbf{B} = Magnetic field in Tesla (N/Amp-m).
- PSD = Power spectral density in $\text{m}^2/\text{sec}^4/\text{Hz}$.
- p = Gas pressure.
- k = Boltzmann constant.
- T = Absolute temperature.
- d_g = Translation damping from residual vacuum.

The proof mass is assumed to be constructed of Osmium which is chosen because of its low electrical conductivity, $\sigma = 1.7 \times 10^6$ mhos/meter, and its high density, 22480 kg/m^3 .

The electric charge is determined by assuming a potential of 0.1 Volt with a gap of 2 cm. The theory of the attraction between a charged sphere and a spherical cavity is developed in [9]. The eddy current theory is developed in detail in SUDAAR 194¹ which is also on the web linked through [1]. It is assumed that the Lorentz force can be shielded by about a factor of 0.1. The angular velocity of the spinning proof mass has been chosen at 1 Hz to keep variations due to proof-mass surface irregularities out of the LISA band.

In calculating the disturbances from the interferometer laser, the reference power of 0.01 watts on the back side of the proof mass was used rather than the beam power from a neighboring satellite which is very small. The value of the laser power fluctuation, of $5 \times 10^{-7} / \text{Hz}^{1/2}$ was taken from [10], page 62, and the value for the interferometer reference power was taken from [11], Section 3.5, page 51. The additional disturbances when the attitude and two axes of a cube are controlled may be seen in [12] and [13].

9. GYRO PERFORMANCE

One of the potential advantages of a spherical proof mass is that it might also be used as a two-axis gyro to improve the pointing performance. There is, however, a major problem in implementing a gyro reference in LISA which will be discussed below. In any event it is necessary to know the stability of the proof mass spin axis. Table 2 shows the calculated drift of a LISA proof mass acting as a gyro. The table was adapted from the relativity-gyro drifts using an unsupported gyro¹⁴. The original calculation considered 24 drift sources, but any drift less than one $\mu\text{as} / \text{yr}$ has been removed from the list. From this table it can be seen that there is only one large drift, eddy currents, so that the total gyro drift is about 0.12 arcsecond per year. This is acceptable for a LISA stabilizing reference.

Source of Torque	Formula for $\dot{\phi}$	Auxiliary Formula, Critical Values, Comments, Etc.	Drift in $\mu\text{as}/\text{yr}$
Gravity Gradient	$\dot{\phi}_{av} = \frac{3}{2} n^2 \left(\frac{\varepsilon_p}{\omega_{PM}} + \frac{k_v \rho_{PM} a^2}{E} \omega_{PM} \right) \theta_{ml}$	$\varepsilon_p = 10^{-4}$	2.49E+01
Magnetic Eddy Currents	$\dot{\phi}_{av} = \frac{\sigma B_{ip\perp} B_{ip\parallel} S_{AC}^2 C_m}{4\rho_{PM}}$	$\sigma S_{AC}^2 C_m = 1.7 \times 10^6 \text{ mhos/m}$	1.24E+05
Barnett Effect	$\dot{\phi}_{peak} = \frac{5\chi_m H_{ip} S_{AC} C_{Bn}}{\rho_{PM} a^2 g_m e/m_e}$	Magnetic susceptibility, $\chi_m = -3.7 \times 10^{-5}$, $S_{AC} C_{Bn} = 1$	1.03E+01
Spinning Charge	$\dot{\phi}_{peak} = \frac{5\varepsilon_0 V(1+a/d) B_e S_{AC} C_{Bn}}{2\rho_{PM} a^2}$	$\dot{\phi}_{s\text{ chg}} = -0.920 \left(\frac{V}{1 \text{ volt}} \right) \dot{\phi}_{Barnett}$	7.09E+00
Gas Brownian Drift	$\langle \phi^2 \rangle = \frac{4b_{Gas} kTt}{h_{PM}^2}$	$b_{Gas} = \frac{8\pi}{3} a^4 p \sqrt{\frac{m_a}{2\pi kT}}$	1.49E+00
Anisotropic χ_m	$\phi_{peak} = \frac{5 \Delta\chi_m B_{ip}^2}{2\mu_0 \rho_{PM} a^2 \omega_{PM}}$	$\Delta\chi_m = 0.1 \chi_m$	4.94E+02
		RSS of all drift sources ($\mu\text{as}/\text{yr}$)	1.24E+05

Table2. Summary of Drift Torque Sources and Drifts

The problem with using the proof mass as a stable two-axis reference gyro is that there is no easy way to read it out. Normally the gyro would be read out by redundant autocollimators shining on optical flats on the north and south poles of the rotor. In the case of LISA the proof-mass spin axis would nominally be aligned perpendicular to the ecliptic. The LISA spacecraft, however, are inclined 60 degrees with respect to the ecliptic and rotate one per year about this axis and about an axis perpendicular to the spacecraft. Thus autocollimators could not be aligned to continuously monitor the gyro spin axis. This is a major unsolved problem for using the proof mass as a two-axis reference.

10. DRIFT CALCULATION NOTATION

A list of the additional notation in Table 2 is:

$\dot{\phi}$	= Gyro drift rate.
n	= Mean orbit rate.
ε_p	= Moment-of-inertia difference ratio.
ρ_{PM}	= Density of the proof mass.
E	= Young's modulus.
k_ν	= $(\nu + 1)(\nu + 2) / (5\nu + 7)$ where ν is Poisson's ratio.
d	= Gap
χ_m	= Magnetic susceptibility.
h_{PM}	= Proof mass angular momentum.
b_{Gas}	= Rotation damping from residual vacuum.
m_a	= Average molecular mass of residual gas.
S_{AC}	= Any magnetic shielding.
V	= Charge potential of the proof mass.

11. CALIBRATING THE SURFACE OF THE SPHERE IF NEEDED

An active damper⁵ makes it possible to calibrate the surface of the sphere. This opens the door to improving the quality of the surface beyond the present value of 20 nanometers by selective polishing or of including the surface calibration in the data reduction.

If a large polhode is commanded in a spherical proof mass spinning either in a drag-free satellite or in a laboratory electric bearing so that the transcollimator scans the entire surface, the surface errors of the sphere can be calibrated. The accuracy of this calibration might be as good as 10^{-12} meters although a more conservative estimate would be 10^{-10} meters, i.e. about one atomic distance. Calibration in space would have no bearing errors, but there now exists well tested theory for the torques acting on a sphere in an electric bearing making laboratory calibration also possible.

In a LISA satellite after calibration was complete, the active damper could drive the spin axis to the maximum axis of inertia; and the sphere would present a known surface to reflecting beams striking its equator to an accuracy of about 10^{-10} meters and perhaps as much as 10^{-12} meters.

12. CONCLUSION

At this point in time a spherical proof mass seems to have several advantages over two single-axis cubes:

- 1) Performance: The acceleration noise of a sphere is approximately 10 times less than a cube, and in fact the free-floating sphere is the best that can be done.
- 2) Heritage: DISCOS has flown, was easy to implement, and has measured the gradients of all fields in its cavity.
- 3) Reliability: The reliability depends on three areas: sensors, control calculations, and thrusters. The last two are essentially the same for either type of proof mass, and the spherical sensors can be made much more reliable by

using 3 or 4 independent 3-axis transcollimators. The reliability should be determined by the above three areas and not by having two masses and two sets of sensing and support electronics.

- 4) Ease of Realization: It was only about 3 years from concept to flight for DISCOS, and it worked perfectly the first time. The subsequent single-axis drag-free satellites took three flights before all of the problems were solved.

In spite of this, these points are not an advocacy for using spheres instead of cubes. Rather they point out the necessity for doing a trade-off study between the two systems including the construction and testing of spherical hardware. This is a very important decision, and it should not be taken unilaterally which seems to be the case at the present time.

REFERENCES

1. Lange, B., www.dragfreesatellite.com, *AIAA Journal*, **2**, 9, p. 1950, 1964. Stanford University Department of Aeronautical Engineering Report (SUDAER) No. 194, Ph.D. Thesis, June 1964.
2. Lange, B., *Managing spherical proof masses in a drag-free satellite with application to the LISA mission*, *Class. Quantum Grav.* **18**, No. 19, pp. 4153-4158, Oct. 2001.
3. Lange, B., *The Two-Color Transcollimator, a Precision Position Detector for a Satellite Two-Sphere Equivalence-Principle Experiment*, Proceedings of the 8th Marcel Grossmann Meeting, Edited by T. Piran and R. Ruffini, p. 1226, 1997.
4. R. V. Jones and J. C. Richards, *J. of Sci. Instr.*, **36**, 2, p 90, 1957. R. V. Jones, *J. of Sci. Instr.*, **38**, 2, p. 37, 1961.
5. B. Parkinson and B. Lange, *J. Spacecr. Rockets*, **7**, 6, p. 667; **7**, 6, p. 675, 1970. B. Lange, *J. Spacecr. Rockets*, **9**, 2, p. 96, 1972.
6. B. Lange, *Drag-free performance in a LISA mission with spherical proof masses*, *Class. Quantum Grav.*, **19**, pp. 1739-1743, April 7, 2002.
7. www.dragfreesatellite.com/discos.html, *APL Technical Digest*, **12**, No. 2, 1973. *J. Spacecr. Rockets*, **11**, 9, p. 637, 1974.
8. Balogh, A. et al., http://helio.estec.esa.nl/uds03/uls_08_a/DOCUMENT/MAG/MAGINST.HTM, Figure 9.
9. Smythe, William R., *Static and Dynamic Electricity*, Third Edition, 5.08, p 128 (Charge forces) and 10.05, p 374 (Eddy currents), Hemisphere Pub. Corp., 1989.
10. LISA Pre-Phase A Report, <ftp://ftp.ipp-garching.mpg.de/pub/grav/lisa/ppa2.09.pdf>, also www.dragfreesatellite.com/lisa.html, linked in paragraph 3.
11. LISA Status Report, ftp://ftp.rzg.mpg.de/pub/grav/lisa/sts_1.04.pdf, also www.dragfreesatellite.com/lisa.html, linked in paragraph 3.
12. Cavalleri et al., *Class. Quantum Grav.* **18**, No. 19, Oct. 2001, pp. 4133-4144.
13. W. J. Weber et al., *Position sensors for LISA drag-free control*, *Class. Quantum Grav.*, **19**, pp. 1751-1756, April 7, 2002.
14. B. Lange, *Design and analysis of a high-accuracy version of the Relativity--Gyro Experiment*, *Phys. Rev. D*, **59**, 102004, May 15, 1999.